Application of Opti-Morph: Optimized beach protection by submerged geotextile tubes

Megan Cook, Frédéric Bouchette, Bijan Mohammadi, Nicolas Fraysse

Application of Opti-Morph: Optimized beach protection by submerged geotextile tubes

Megan Cook[1,3,*], Frédéric Bouchette[1], Bijan Mohammadi[2], Nicolas Fraysse[3]

Abstract

This paper illustrates the potential of Opti-Morph, a new morphodynamic model based on wave-energy minimization driven morphodynamics. Given the fast simulation times, this model is ideal for determining the optimal position of submerged breakwaters to maximize efficiency. This paper focuses on the study of the location of submerged geotextile tubes for optimal beach protection, while taking into account the evolution of the seabed.

Keywords: coastal engineering, Opti-Morph, optimization, breakwater

1. Introduction

The question of coastal protection is of crucial importance, and breakwaters are a typical example of means to approach this. Designed to absorb/dissipate the energy of incoming waves and therefore reduce coastal erosion, breakwaters date back to the Roman Empire and have been used for coastal protection ever since [1]. Different types of breakwaters exist depending on whether they are emerged, floating [2] or submerged [3]. Examples include rubble-mound, caissons, pontoons, and geosynthetic tubes. The nature of the considered breakwater depends on many factors such as wave conditions, water depth, characteristics of the seabed foundations, cost

*Corresponding author

Email addresses: megan.cook@umontpellier.fr (Megan Cook), frederic.bouchette@umontpellier.fr (Frédéric Bouchette), bijan.mohammadi@umontpellier.fr (Bijan Mohammadi), nicolasfraysse@brl.fr (Nicolas Fraysse)

[1]GEOSCIENCES-M, Univ Montpellier, CNRS, Montpellier, France

[2]IMAG, Univ Montpellier, CNRS, Montpellier, France

[3]BRL Ingénierie, Nîmes, France

of construction and maintenance, as well as visual and environmental impacts. Different characteristics of the breakwater need to be studied. This includes length and width of the structure, orientation, and location with regard to the shoreline, shape. Given the many parameters surrounding the design of breakwaters, i.e. length, width, shape, location, orientation, etc., it is natural to consider numerical simulations to accompany the investigation.

This paper details the numerical study of submerged breakwaters made of geotextile material. For the sake of simplicity, this study focuses on one breakwater parameter: its location along the cross-shore profile. The objective is to determine the optimal position of a geotextile tube for minimal beach erosion along the cross-shore profile and to do so, optimization methods are required.

The use of optimization methods for coastal protection can easily be found in the literature, such as [4, 5] for the protection of ports, [6, 7] in the case of the design of seawalls, and [8, 9, 10] for the study of breakwaters. Geotextile tubes, or geotubes, have already been the subject of an optimization study on a static background [11, 12], where the authors sought the optimal shape of these coastal protection structures. Here, we search for the optimal location of the seabed, while taking into account the morphodynamic response of the seabed, the latter being determined by the numerical model, Opti-Morph [13].

Opti-Morph is a new morphodynamic model, based on the theory that shallow-water seabeds react to the surface waves and evolves in an effort to minimize a certain hydrodynamic quantity. This concept was first formulated in the works of [14, 15, 16, 17], in a somewhat theoretical context. The numerical model Opti-Morph was then developed (cf. [13]), in an effort to apply this concept to experimental and in situ configurations and validate the theory. Advantages of this numerical model include its low number of hyperparameter and their robustness, its fast simulation times. The work of [13] demonstrates the potential of this up-and-coming morphodynamic model, with both short-term and long-term simulations.

This paper presents the potential of this new morphodynamic model, by applying it to the problem of the positioning of submerged geotextile tubes. First, we define the optimization problem regarding the position of the breakwater for optimal coastal protection, with the definition of the domain, the objective function, and constraints. Next, we offer a brief description of the Opti-Morph model, which is based on wave energy optimization and thus requires the definition its own cost function. A description of the coupling of

both optimization problems is approached in section 4 before presenting the numerical results.

2. Geotube Position Optimization

2.1. Description

Geotextile tubes are made from high-strength geosynthetic fabric and are increasingly used in coastal and riverine applications. They are often filled hydraulically with a slurry of sand and water, although many other materials have been used. Sand-filled flexible tubes of geotextile material are used for their ability to allow water to pass through but maintain the sand within. Geotextiles tubes are for coastal protection by the means of revetments, protection dykes, groynes, and offshore breakwaters [18, 19], the latter being the focus of this study. Like other types of offshore emerged breakwaters, geotextile tubes are designed to dissipate the waves by creating local shallow water conditions forcing waves to prematurely break, thus, ensuring less energy arrives at the coast and in doing so protecting the shoreline from erosion. Geotextile tubes have been deployed all over the world, on account of their low costs and less ecological and environmental impact [20, 21], having little effect on the local marine fauna and flora. Their easy installation and maintenance, with potentially locally sourced materials and their low visual impact also play a role in their increasing popularity.

One such example is the introduction of submerged geotextile breakwaters on the Northern coast of Yucatan, Mexico [22, 23]. Beaches were sustaining erosion of approx. $1\,m$ per year, with many beaches being almost fully eroded. Several geotextile tubes were installed $10\,m$ and $30\,m$ from the shoreline with promising results. Similarly, geotextile tubes were deployed for the coastal protection of Young-Jin beach on the east coast of Korea [24, 25]. The situation was so critical shoreline roads and other public properties were being damaged. Eight geotubes tubes were deployed along the beach at $90\,m$–$100\,m$ from the shoreline, with a water depth of $3\,m$. Field monitoring shows an extension of up to $7.6\,m$ of the shoreline and an accumulation of sand around the areas covered by the geotextile tube. On the Lido of Sète, France, on the Mediterranean Sea, submerged geotextile tubes were also installed [26, 11]. Here, they were deployed approximately $350\,m$ from the beach with a depth of $4\,m$ and induced an important enlargement of the beach. Extensive studies were made prior to the installation. In particular, the location of the geotubes with regards to the coastline. In the three

previous examples, the position of the structures ranges between $10\,m$ and $350\,m$ from the shore.

Here, we study the optimal location of the geotube using a numerical model. To do so, we must define the quantity to be minimized as well as the physical constraints that arise.

2.2. Geotube Deployment Objective Function

The search for the optimal geotube location depends on the choice of the cost function, or objective function to be minimized or maximized. Several cost functions can be considered depending on the main objective of the deployment, whether it's environmental, financial or physical (e.g. limiting beach erosion or reducing wave energy). It may also be a combination of several factors. In this study, we seek to minimize the position of the shoreline, in order to prevent erosion and encourage accretion. For illustrative purposes, we consider one geotube parameter, its location along the cross-shore profile, but additional parameters can be incorporated if desired.

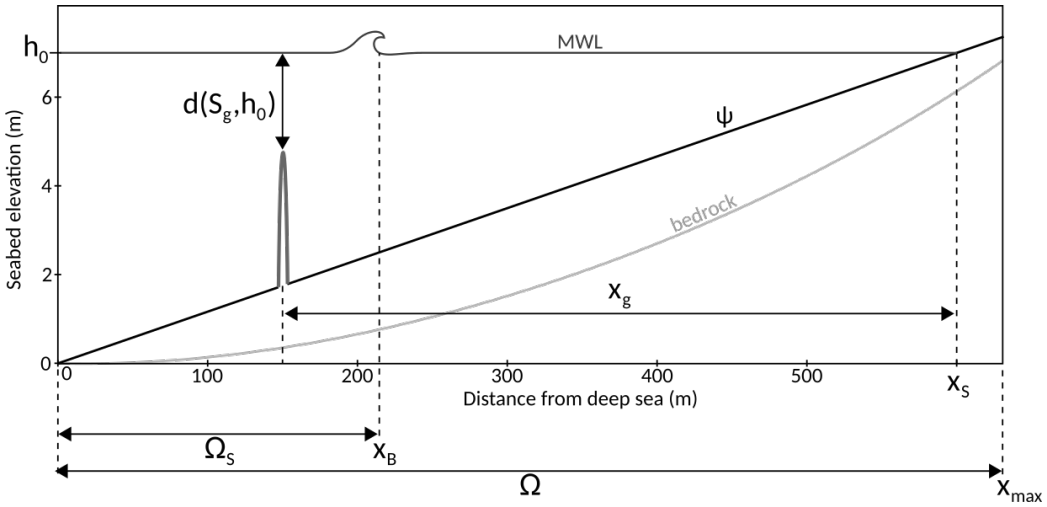

Figure 1: Diagram of the cross-shore profile featuring a geotube

Let $\Omega = [0, x_{\max}]$ be the domain of the cross-shore profile, where $x = 0\,m$ is an arbitrary point situated in deep waters and $x_{\max}$ is a point located beyond the shoreline, as shown in Figure 1. Let ψ be the elevation of the seabed, and $x_{\mathrm{G}} \in \Omega_{\mathrm{G}}$ the location of the geotube, where Ω_{G} is the zone of feasible deployment. We define the geotube deployment objective function as the final position of the shoreline $x_{\mathrm{S}} \in \Omega$:

$$\mathcal{J}_{\mathrm{G}}(x_{\mathrm{G}}) = x_{\mathrm{S}}(t = T, x_{\mathrm{G}}) \qquad (m) \tag{1}$$

where $[0, T]$ is the time interval considered for the morphodynamic response. This function is to be minimized in the search of the optimal geotube location.

2.3. Constraints

Certain constraints associated with the introduction of geotextile tubes need to be considered in the search for the optimal position. These constraints are used to exclude certain positions which are deemed unacceptable. For instance, geotextile tubes cannot be installed in too deep a water because the deployment of such a structure, as well as its maintenance, will prove to be too difficult and expensive. The topography of the seabed may also limit the choice of position, with sharp rock or debris that may damage the tubes. Protected marine flora may also restrict the feasible zones of deployment. Furthermore, one should avoid installing geotextile tubes in shallow waters where they risk being damaged by beach users, in particular the keels of ships which can cause lesions to the geotextile material.

As such, in this study, we impose that the geotextile tubes must be set: (i) close enough to the shore to allow for easy deployment/maintenance; (ii) such that the vertical distance between them and the water surface measures at least $1\,m$. For illustrative purposes, topographical constraints have not been included, but can easily be added if necessary.

3. Morphodynamic Response by Wave Optimization

3.1. Description

Opti-Morph is a new hydro-morphodynamic model developed to simulate the dynamics of sandy beaches and designed to be robust, of low complexity, and have remarkably low execution times. For this reason, Opti-Morph is a natural choice of morphodynamic model regarding problems relating to coastal engineering. This model, first presented in [13] is used here in the study of the optimal location of geotubes. The central theory behind the Opti-Morph model is the assumption that the seabed evolves naturally in an attempt to minimize the energetic state of the surface waves. This is achieved through the minimization of a hydro-morphodynamic cost function, this minimization is deemed the driving force behind the morphodynamic response.

Constraints are added to the model for increased realism; phenomena that are secondary to the morphodynamic processes are considered constraints.

3.2. Hydro-morphodynamic Cost function

The hydro-morphodynamic cost function driving the Opti-Morph model is the same as that of [13], i.e. the potential energy of shoaling waves:

$$\mathcal{J}(\psi, t) = \frac{1}{16}\int_{\Omega_S} \rho_w g H^2(\psi, x, t)\mathrm{d}x \qquad (J.m^{-1}) \tag{2}$$

for all $t \in [0, T]$, where Ω_S is a time-dependent subset of Ω over which the waves shoal (see Figure 1), H denotes the height of the waves over the cross-shore profile (m), ρ_w is water density $(kg.m^{-3})$ and g is the gravitational acceleration $(m.s^{-2})$.

3.3. Constraints

In the works of [13], two constraints are mentioned: (i) a sandstock constraint, which ensures that the quantity of sand in a closed basin remains constant over time and (ii) a slope constraint preventing the seabed from being unrealistically steep. In the aforementioned work, Opti-Morph was applied to a flume configuration and thus required the presence of a sandstock constraint to guarantee that the quantity of sand remains constant over time. Given the open-sea setting of this study, a sandstock constraint is not required but is used here to limit the displacement of sand between the deep waters and the nearshore zone. The slope constraint remains the same, with a limit of the slope of the seabed by a quantity relative to the critical angle of repose of the sediment. This constraint prevents impossibly steep slopes from forming, which would lead to unrealistic results.

4. Coupling

Two optimization problems have been defined and must be resolved simultaneously: the geotube positioning along the cross-shore profile and the morphodynamic response of the seabed performed by Opti-Morph. This requires special treatment for their resolution.

4.1. Optimization problem 1: Geotube Positioning

The first optimization problem concerns the optimal geotube position. This can be formulated as follows:

(P1): Find $x_G \in \Omega_G$ *such that* $\mathcal{J}_G(x_G)$ *defined by* (1) *is minimal and subjected to two constraints:*

- *(C1):* $x_G < x_G^{max}$
- *(C2):* $d(S_G, h_0) < 1$

where $x_{\mathrm{G}}^{\max}$ (m) is the maximal distance from the coast for geotube deployment, and $d(S_{\mathrm{G}}, h_0)$ (m) is the distance between the summit of the geotube S_{G} and the mean water level h_0 (cf. Figure 1).

Constraint $(C1)$ prevents the geotube from being installed too far from the coast : geotubes cannot be deployed beyond a distance of $x_{\mathrm{G}}^{\max}$ from the coast. Constraint $(C2)$ ensures that the geotube is located deep enough to evade collision with boats and other beach users which could potentially damage the tubes. Here, a minimum of $1\,m$ is permitted between the geotube and the water surface.

4.2. Optimization problem 2: Morphodynamic Response of the Seabed

The second optimization problem determines the evolution of the shape of the seabed over the course of the simulation and can be summarized as:

(P2): For each $t \in [0, T]$*, find* $\psi \in \Psi$ *such that* $\mathcal{J}(\psi, t)$ *defined by* (2) *is minimal and subjected to the constraints:*

- *(C1'):* $\displaystyle\int_\Omega \psi(t, x)\,dx = \int_\Omega \psi(t = 0, x)\,dx \qquad \forall t \in [0, T]$
- *(C2'):* $\displaystyle\left|\frac{\partial \psi}{\partial x}\right| \leq M_{slope}$

where Ψ is the set of physical parameters describing the characteristics of the seabed and M_{slope} is a grain-dependent upper-bound of the seabed slope.

The constraint $(C1')$ and $(C2')$ describe the constraints mentioned in Section 3.3. The first is the sandstock constraint, which limits the sediment transfer between the nearshore zone and the deep sea. This is achieved by setting the sandstock as constant over the course of the simulation. Constraint $(C2')$ ensures that the slope of the seabed cannot be overly steep by defining the upper-bound M_{slope}.

4.3. Workflow

Given the low run time and complexity of Opti-Morph to solve ($P2$), it is possible to solve ($P1$) using a direct optimization method. Other optimization methods such as a gradient descent method can be applied, if the morphodynamic model used is more complex and if only a small number of morphodynamic simulations can be performed. This study operates in a manner analogous to the search for an optimal port configuration in [5], but the morphodynamic response of the sandy seabed is now incorporated in the study.

Before launching the simulation, the parameterization of the Opti-Morph model must be defined, including the domain of the cross-shore profile Ω, the initial seabed $\psi_{|_{t=0}}$, the forcing conditions, and the parameters determining constraints. The set of all considered geotube positions must also be provided. For each position of geotubes, the morphodynamic response is calculated over time. The geotube deployment objective function $\mathcal{J}_{\mathrm{G}}$ is then deduced. When the set of eligible positions has been explored, the value of x_{G} which minimizes $\mathcal{J}_{\mathrm{G}}$ can then be determined. An explanatory diagram of the implementation strategy is given in Figure 2.

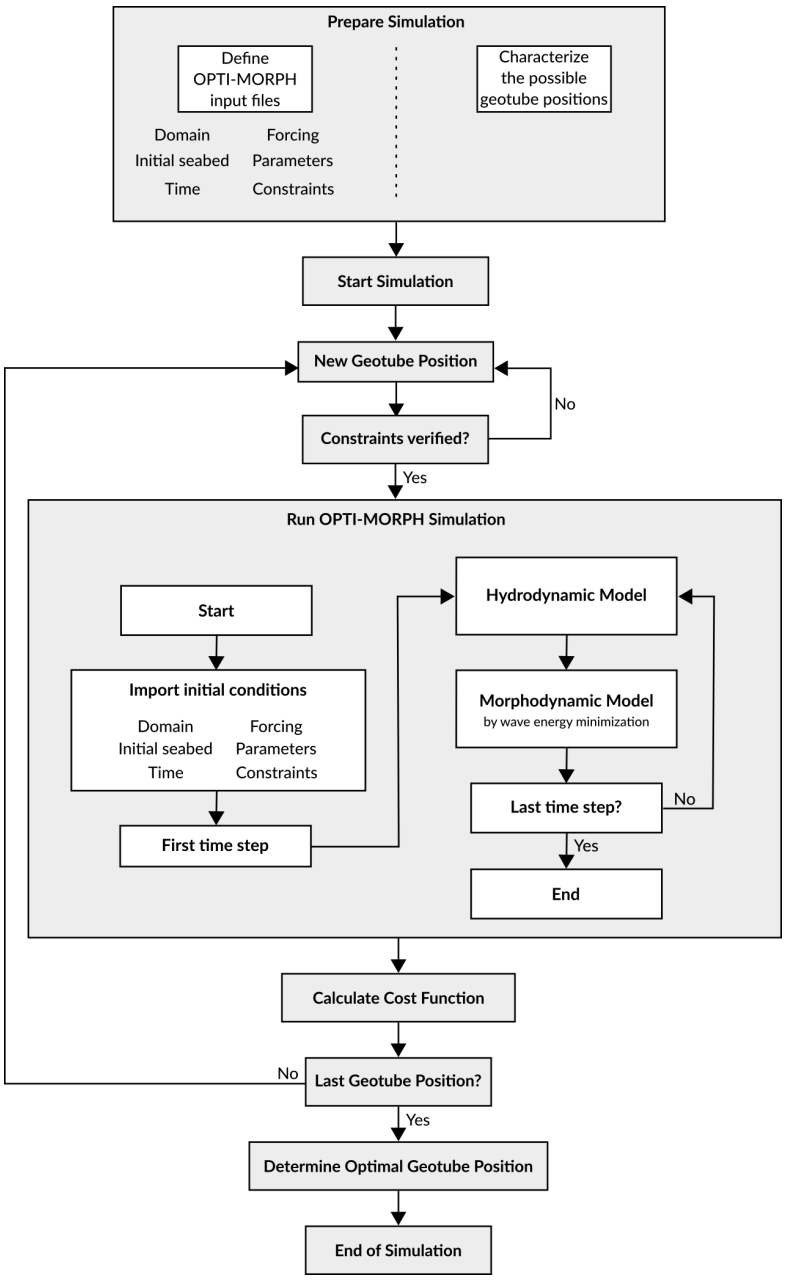

Figure 2: Diagram of the structure of the model capable of finding the optimal geotube position while incorporating the morphodynamic response of the seabed.

5. Application and Numerical Results

5.1. Setting

For simplicity, this study concerns a 1D cross-shore beach profile, although it can be easily adapted to the 2D case, once Opti-Morph has been extended to cater to 2 dimensional configurations. The initial seabed is a linear seabed measuring $600\,m$ along cross-shore profile, similar to the seabed at Sète, France [26]. Bedrock features in the configuration as shown in Figure 1. The domain of the cross-shore profile is subdivided into $1\,m$ long cells, allowing for a horizontal precision of $1\,m$ over the $600\,m$ domain. The mean water level (MWL) is set at $7\,m$. We consider a simple 20-day forcing scenario characterized by a rise-peak-fall storm over 6 days and fair weather conditions preceding and succeeding the storm. The sediment is considered fine sand with a critical angle of talus of 0.2. Geotubes are to be placed along the cross-shore and are defined by a width of $6\,m$ and a height of $3\,m$. Constraints of problem $(P1)$ restrict the deployment of the geotextile tube to the interval $x_{\mathrm{G}} \in (350, 495]$.

5.2. Results

This section is devoted to the numerical results of both optimization problems: the search for the optimal position of the geotube for minimal coastal erosion and the natural morphodynamic response of the seabed.

Figure 3.A illustrates the variations of the geotube deployment objective function $\mathcal{J}_{\mathrm{G}}$ defined by Equation (1), with regard to the location of the geotube. We observe a piecewise constant function with erosion ranging between $2\,m$ for $x_{\mathrm{G}} = 351$ and $9\,m$ for $x_{\mathrm{G}} = 495\,m$. The optimum is located in the zone nearest the coast, over the $351\,m$-$388\,m$ plateau. As such, geotubes located anywhere between $351\,m$ and $388\,m$ from the coast induce the same retreat of the shoreline of $2\,m$. Given the downward trend of the objective function, it is natural to elect $x_{\mathrm{G}} = 351\,m$ as the optimum for the remaining studies. The piecewise constant nature of the objective function is due to the $1\,m$ precision of the discretization of the cross-shore domain Ω.

Figure 3.B illustrates the morphodynamic response of the seabed in relation to the different positions of the geotube. Four simulations were performed, with geotubes located at $x_{\mathrm{G}} = 495\,m$ (blue), $x_{\mathrm{G}} = 450\,m$ (green), $x_{\mathrm{G}} = 400\,m$ (yellow), and $x_{\mathrm{G}} = 351\,m$ (red), where the latter corresponds to an optimal geotube position. The value of the objective function $\mathcal{J}_{\mathrm{G}}$ associated with each of the geotubes is labeled in Figure 3.A. A fifth simulation

was also performed without geotube (black) for the purpose of providing a reference in the efficiency analysis of the geotubes.

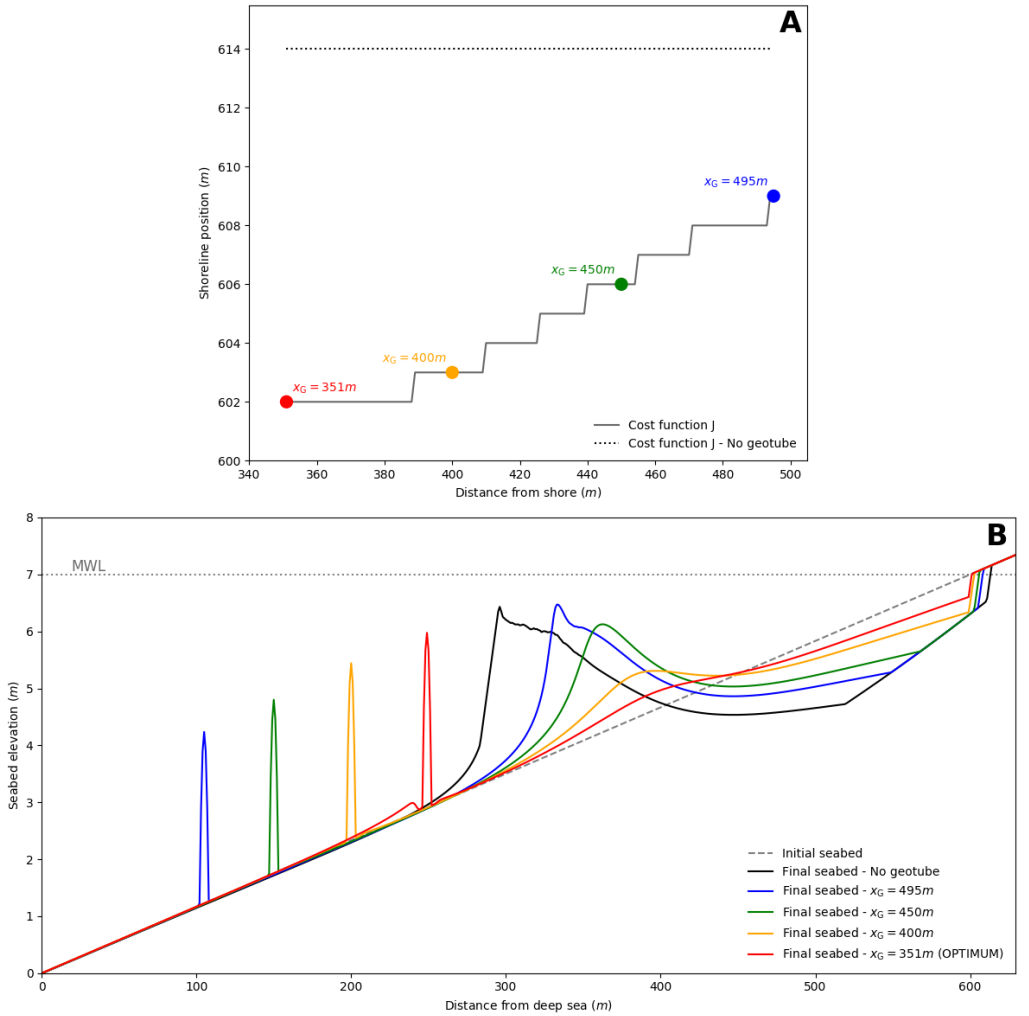

Figure 3: Results of the numerical search of the optimal geotube position via Opti-Morph. **A.** Variations of the geotube deployment objective function with regards to the distance between the geotube and the shoreline. The objective function calculated over a cross-shore profile with geotubes is also given as a reference. Four points are emphasized, corresponding to the four seabeds depicted in the second graphic. **B.** Final seabed profiles produced by the morphodynamic model Opti-Morph with varying geotube positions over the cross-shore profile.

At the end of the numerical simulation, each seabed features a sandbar, the height and location of which depend on the geotube position. A sandbar located at $x = 330\,m$ appears for a geotube deployed at $x_{\mathrm{G}} = 495\,m$ (blue) with a height of $2.6\,m$. The closer the geotube is to the shoreline, the smaller and closer the resulting sandbar is to the coast. For a geotube located $450\,m$ (green) from the shoreline, the resulting sandbar measures $1.9\,m$ and is located at $x = 360\,m$. For a geotube at $x_{\mathrm{G}} = 400\,m$ (yellow), the sandbar measures $0.8\,m$ in height, and for $x_{\mathrm{G}} = 351\,m$ (red), it measures $0.3\,m$. The latter two are located at $x = 390\,m$. A trough proportional to the sandbar has also appeared near the coastline, and induces erosion at the coast. Limited by the bedrock, this trough has a depth of $1.1\,m$ for $x_{\mathrm{G}} = 495\,m$ and $0.4\,m$ for $x_{\mathrm{G}} = 351\,m$. The greatest displacement of sediment is observed for a seabed devoid of geotubes. A sandbar located at $x = 300\,m$ appears with a height of $3\,m$, as well as a $1.3\,m$ deep trough.

Opti-Morph is capable of producing realistic results when dealing with submerged breakwaters. Indeed, the closer the geotube is positioned relative to the coast, the more wave energy is dissipated, and as such less seabed movement can be observed. For $x_{\mathrm{G}} = 351\,m$, i.e. the optimal geotube, very little movement occurs, whereas for $x_{\mathrm{G}} = 495\,m$, the shape of the seabed has undergone major transformation. Conversely, the further in deep waters the geotube is deployed, the more the seabed behaves as if no geotube has been introduced. This is due to the fact that in too deep a water, the geotube have little effect on the surface waves, allowing waves to pass with little to no attenuation, and as such, he energy hitting the shore is comparable to a configuration without geotubes. This can be observed by the final shape of the sandbar and trough for the deeper geotubes compared to the non-geotube configuration.

Furthermore, 3.B shows that the position of the geotube has a noticeable effect on the shoreline, with the red geotube inducing less erosion than those situated further seaward. This can be explained by the decrease of wave energy associated with the geotubes nearer the shore. According to Figure 3.A, deploying a geotube anywhere in the $[105, 250)$ zone has a positive effect on the shoreline, when compared to that without geotubes. Indeed, even in the worst case, with a geotube situated at $x_{\mathrm{G}} = 495\,m$, the objective function is lesser ($\mathcal{J}_{\mathrm{G}}(x_{\mathrm{G}} = 495) = 609\,m$) than without any geotubes where the objective function is $614\,m$.

We notice an accumulation of sand at the foot of the $x_{\mathrm{G}} = 351\,m$ geotube. The small trough is due to numerical inaccuracies; further developments are

required on Opti-Morph to allow sand to build up against the solid structure. However, this accumulation of sand seaward of a geotube is often encountered in in situ observations of the behavior of the seabed following the deployment of a submerged breakwater [27].

6. Discussion

6.1. Effect of the Geotube on Wave Height

In this section, we analyze the behavior of the hydrodynamic model used by Opti-Morph. Figure 4 shows the height of the waves over the cross-shore profile at three different points in time: (i) after 2 days (Fig. 4.A) to observe the wave height during fair-weather conditions before the storm, (ii) after 8.3 days (Fig. 4.B) at the peak of the storm, and (iii) 18.7 days (Fig. 4.C) after the storm has occurred and the fair-weather conditions have returned. For each of the three points of time, the wave height associated to five different morphodynamic configurations is depicted. Black shows the wave height associated to a seabed without geotube. The blue, green and yellow profiles show the wave height corresponding to a seabed where a geotube has been deployed at $x_{\mathrm{G}} = 495\,m$, $x_{\mathrm{G}} = 450\,m$ and $x_{\mathrm{G}} = 400\,m$ respectively, and the red corresponds to the optimal geotube position, for $x_{\mathrm{G}} = 351\,m$.

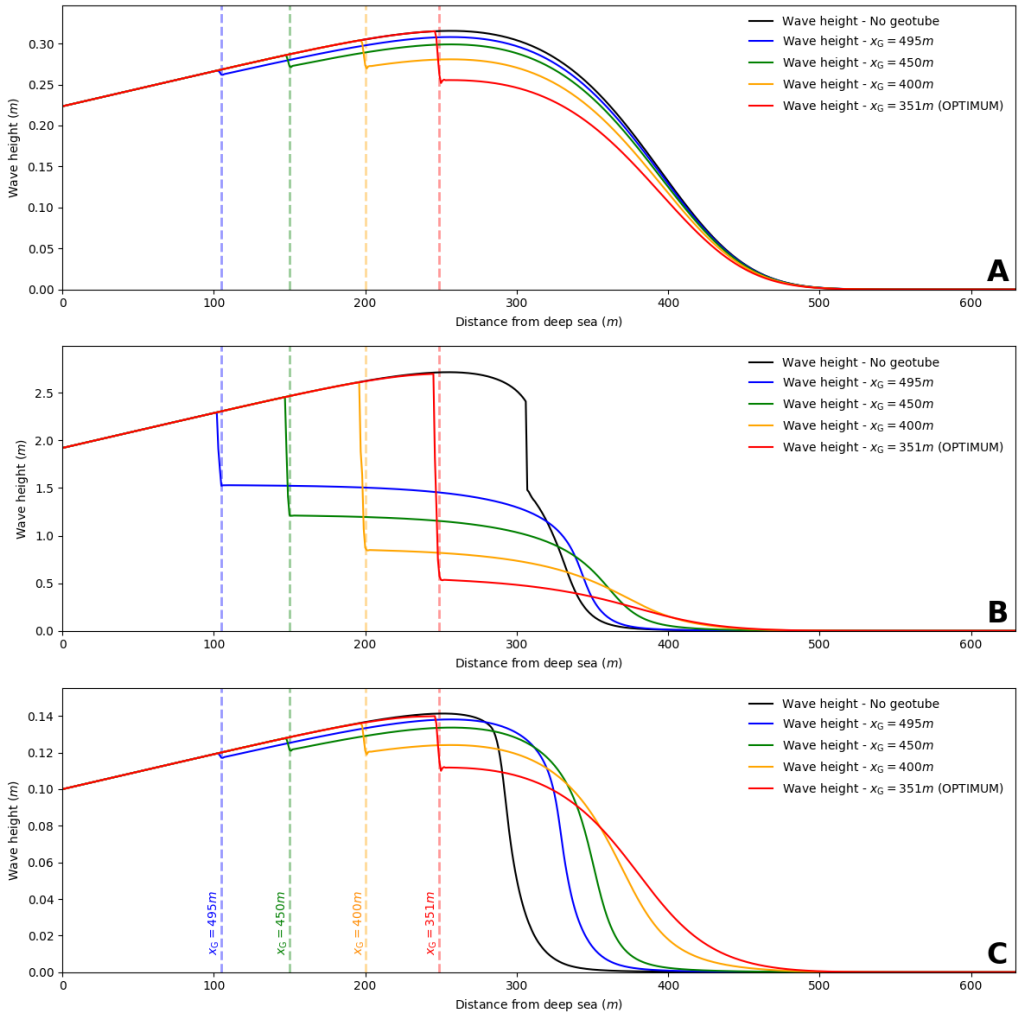

Figure 4: Wave height over the cross-shore profile associated with four geotube positions: $x_G = 495\,m$ (blue), $x_G = 450\,m$ (green), $x_G = 400\,m$ (yellow), and $x_G = 351\,m$ (red). Wave height relating to a seabed profile devoid of geotubes has also been given as a reference (black). **A.** Wave height prior to the storm at $t = 2\,days$. **B.** Wave height at the apex of the storm at $t = 8.3\,days$. **C.** Wave height posterior to the storm at $t = 18.7\,days$.

Figure 4 demonstrates that the simple hydrodynamic model used by Opti-Morph is capable of handling underwater breakwaters, as shown by the fact that the waves behave as expected: (i) waves shoal prior to the geotube with an increase in wave height, (ii) geotubes trigger a breaking effect on the waves with a sharp drop of height, and (iii) after breaking, wave height decreases

smoothly before reaching the coast. Furthermore, Figure 4 illustrates the different impact that geotubes have on the surface waves depending on the height of the latter. Indeed, we observe that geotubes have little impact on the small waves of Figures 4.A, and 4.C, with a drop of a few millimeters, whereas when the wave height is great, as in Figure 4.B, the drop can reach up to $2\,m$ (red). This behavior of the wave height is characteristic of cross-shore profiles containing a geotube.

In addition, geotubes in deeper waters have less effect on the waves as those in shallower waters. In Figure 4.B, the geotube located at $x_{\mathrm{G}} = 495\,m$ induces as drop of $0.8\,m$ whereas the optimal geotube, located at $351\,m$ provokes a drop of over $2\,m$. This can also be illustrated using the transmission coefficient, K_{t}, described in [28, 19] as the ratio between the height of the waves prior to the geotube and posterior to the geotube, and used to describe the efficiency of submerged breakwaters. This coefficient ranges between 0 and 1, where 0 indicates no transmission (i.e. an impermeable structure) and 1 indicates complete transmission (i.e. the geotube has no impact on the surface waves). According to [19], a transmission coefficient lesser than 0.6 is required for the most effective submerged breakwaters.

At the apex of the storm, the optimal geotube has a transmission coefficient of $K_{\mathrm{t}} = 0.20$. Geotubes located at $x_{\mathrm{G}} = 495\,m$, $x_{\mathrm{G}} = 450\,m$ and $x_{\mathrm{G}} = 400\,m$ have a transmission parameter of $K_{\mathrm{t}} = 0.68$, $K_{\mathrm{t}} = 0.49$ and $K_{\mathrm{t}} = 0.32$ respectively. In fact, K_{t} is inferior to 0.6 for all geotubes located between $351\,m$ and $475\,m$ from the coast. In other words, geotubes deployed beyond the $x = 475\,m$ threshold from the shoreline are deemed ineffective in reducing wave energy.

6.2. Time-dependent Geotube Analysis

The main purpose of introducing a geotube to the cross-shore profile is to provoke premature breaking of the greater waves, and thus reducing the energy of the waves and limiting coastal erosion. As such, this section is devoted to the analysis of these three physical quantities. Figure 5 shows the influence of geotubes on the breaking location, the energy of the waves, and the shoreline.

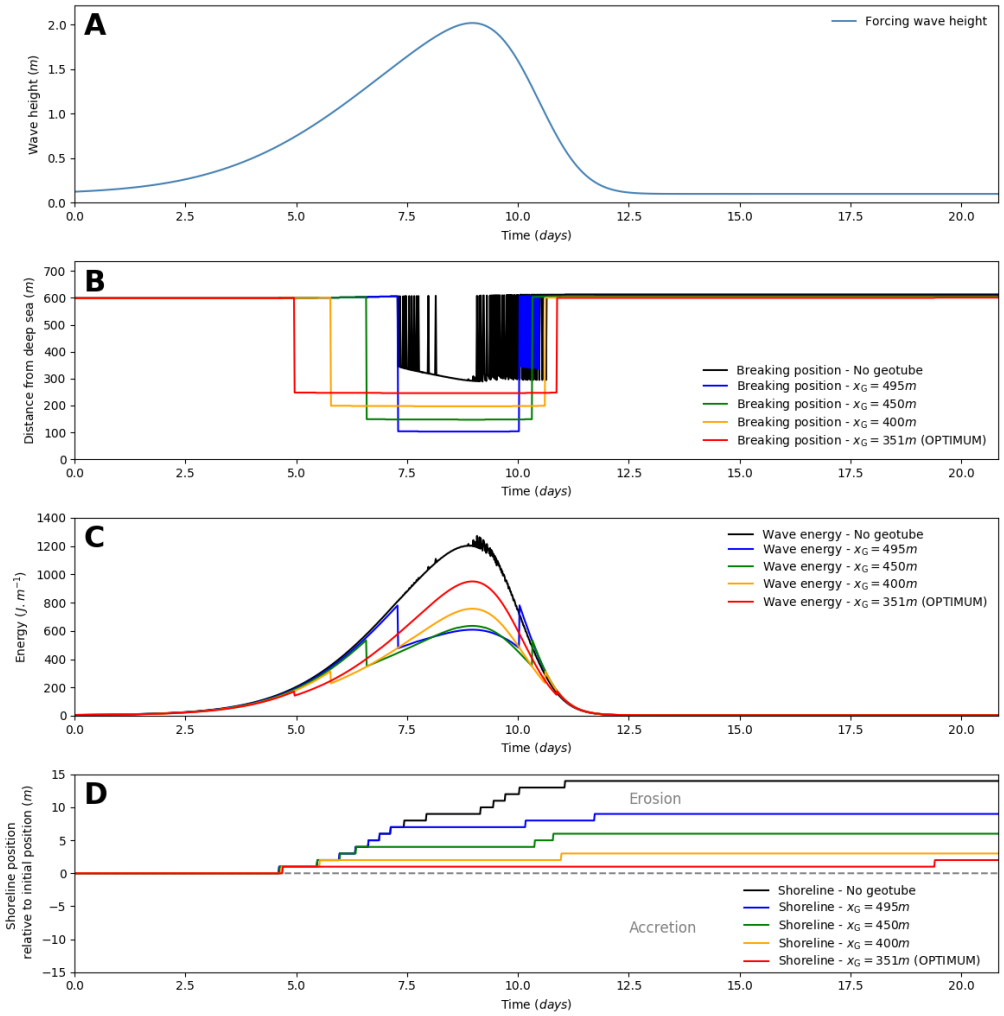

Figure 5: Time series of the wave breaking position, wave energy and shoreline position for different geotube configurations : $x_G = 351\,m$ (red), $x_G = 400\,m$ (yellow), $x_G = 450\,m$ (green), and $x_G = 495\,m$ (blue). The time series of the forcing wave height is also provided. **A.** Forcing wave height. **B.** Time series of the wave breaking position associated with different geotube locations. Should several breakings occur, the first event is retained. The breaking position associated to a seabed devoid of geotubes is also given (black). **C.** Time series of the energy of the waves associated with different geotube locations. The energy associated to a seabed devoid of geotubes is also given (black). **D.** Time series of the position of the shoreline relative to its initial location at $x = 600\,m$, and associated with different geotube locations. A positive value indicates erosion and a negative value indicates accretion. The breaking position associated to a seabed devoid of geotubes is also given (black).

Figure 5.A shows the time-series of the forcing wave height in order to identify the different forcing conditions exerted on the beach profile. We can then analyze the effect of the storm on the breaking waves, energy, and shoreline position. Forcing wave height follows a Gaussian curve, the peak appearing at $t = 9$ days. After day 13, fair weather conditions return for the remaining 8 days of simulation. Figures 5.B, 5.C, and 5.D respectively show the evolution of the breaking point, energy of the waves, and shoreline associated with this forcing scenario, for seabeds without a geotube (black), with a geotube located at $x_{\mathrm{G}} = 351\,m$ (red), $x_{\mathrm{G}} = 400\,m$ (yellow), $x_{\mathrm{G}} = 450\,m$ (green), and $x_{\mathrm{G}} = 495\,m$ (blue).

Figure 5.B shows the evolution of the breaking point of the waves over the course of the simulation. All five profiles show breaking occurring at the coast at the beginning and end of the simulation, i.e. when the forcing wave height is minimal. This result is normal given that geotubes are expected to have little effect on smaller waves and greater effect on larger ones. In the case of the optimal geotube (red), we observe that breaking occurs at the site of the geotube (i.e. $x_{\mathrm{G}} = 351\,m$) at day 5, and continues to break there up until day 11, that is when the forcing wave height exceeds $0.75\,m$. The geotube placed at $x_{\mathrm{G}} = 400\,m$ (yellow) induces wave breaking as of day 5.8 and continues to do so until day 10.6; this corresponds to a forcing wave height exceeding $1\,m$. Similarly, the geotube placed at $x_{\mathrm{G}} = 450\,m$ (green) induces wave breaking over the 6.5 - 10.3 day interval, which corresponds to a forcing wave height exceeding $1.2\,m$. Finally, in a configuration with a geotube placed at $x_{\mathrm{G}} = 495\,m$ (blue), wave break at the site of the geotube from day 7.3 until day 10, when the forcing wave height exceeds $1.5\,m$. For another 0.5 days, waves breaking fluctuates between $340\,m$ and the shoreline. This corresponds to the sandbar which appeared over the course of the simulation as shown in Figure 3.B, and now acts as a natural submerged breakwater, prematurely breaking the waves before they hit the coast. This phenomenon is more observable for the configuration with no submerged structures (black). Here, breaking occurs at the coast up until day 7.3. Then, waves breaks at $x = 350\,m$, due to the appearance of the sandbar, which acts as a natural breakwater. Breaking continues to occur around this point, fluctuating often with the coast. Over the course of the simulation only 12% of the waves break away from the shoreline.

Figure 5.C shows the evolution of the energy of surface waves over time, given by $E = \frac{1}{16}\int_{\Omega} \rho g H^2 \mathrm{d}x$ $(J.m^{-1})$. Before and after the geotubes take effect, all four energy profiles coincide with the energy profile associated with

no geotubes. However, we observe a drop in energy when the wave height is sufficiently high to detect the geotube, i.e. at day 5 for the optimal geotube (red), day 6.5 for the geotube located at $x_G = 450\,m$ (green), day 5.8 for $x_G = 400\,m$ (yellow) and day 7.3 for the geotube located at $x_G = 495\,m$. Similar observations can be made after the storm peak, with a sharp rise of energy when the geotubes no longer affect the waves.

Energy reaches $1240\,J.m^{-1}$ at the apex of the storm in the case of no geotubes. This has been significantly reduced for all the geotube simulations. In fact, the geotube located at $x_G = 351\,m$ (resp. $400\,m$, $450\,m$ and $495\,m$) generates an apex energy of $950\,J.m^{-1}$ (resp. $755\,J.m^{-1}$, $635\,J.m^{-1}$ and $610\,J.m^{-1}$), this suggest a reduction of energy of $290\,J.m^{-1}$, $485\,J.m^{-1}$, $605\,J.m^{-1}$, and $630\,J.m^{-1}$ respectively.

Figure 5.D depicts the evolution of the shoreline. The shoreline remains constant over the first 4.6 days of the simulation, when the forcing wave height remains small ($0.6\,m$). The seabeds with geotubes closest to the shore experience relatively little erosion, varying from its initial position by $2\,m$ for $x_G = 351\,m$ and $3\,m$ for $x_G = 400\,m$. The greater the distance between the geotube and the shoreline, the greater the erosion. For $x_G = 450\,m$, we observe a retreat of $6\,m$ and $9\,m$ for $x_G = 495\,m$. In the case of no geotubes, the shoreline experiences the greatest retreat with a variation of $14\,m$. Once the storm has passed, and the height of the forcing waves is once again small, the shoreline remains stable over the subsequent period of the simulation.

Figure 5 shows unsurprising results when it comes to the influence of the geotubes on the breaking position, wave energy, and shoreline position, and demonstrates the potential of Opti-Morph. This model, with a simple approach to hydrodynamic processes, illustrates several phenomena one would expect of a geotube deployment. First, Figure 5.B shows that waves pass over the geotubes smoothly for smaller waves. Also, the further the geotube is from the coast, the greater the waves have to be for the geotube to take effect. When a geotube is detectable, breaking occurs directly above, demonstrating that it is the submerged breakwater which causes the premature breaking. Figure 5.C shows that any geotube capable of prematurely breaking the waves causes a reduction of energy. We observe that the geotube reducing the most energy is not the same as the one obtained during the optimal search (red). Based on this observation, we investigate which geotube location minimizes wave energy in the following section. Finally, 5.D demonstrates that premature breaking has a positive effect on the shoreline; breaking away from the coast over a long period of time leads to less erosion

at the coast.

6.3. Alternative Geotube Deployment Objective Function

The adaptability of this approach in the search of the optimal geotube position is illustrated in this section. We perform the previous analysis, with the same constraints and forcing conditions, but using a different geotube deployment objective function. The choice of cost function will depend on many factors, and as such flexibility with regard to its choice is preferred. Previously, the search of the optimal position is performed with regard to the position of the shoreline (cf. Eq. (1)). In this section, we choose to minimize the time-averaged energy of the surface waves, as mentioned in Section 6.2 and in Figure 5, where it was revealed that an optimal geotube in terms of minimal erosion is not necessarily equivalent to an optimal geotube in terms of energy.

Given that the geotextile tubes are designed to prematurely cause wave breaking and thus ensuring less energy arrives at the coast, in this study we seek to minimize the cumulative energy of the waves over the cross-shore profile.

As such, a new objective function is considered:

$$\tilde{\mathcal{J}}_{\mathrm{G}}(x_{\mathrm{G}}) = \frac{1}{16}\int_0^T \int_\Omega \rho g H^2(x,t,x_{\mathrm{G}})\mathrm{d}x\mathrm{d}t \qquad (J.m^{-1}.s^{-1}) \tag{3}$$

where ρ is water density ($kg.m^{-3}$), g is gravitational acceleration ($m.s^{-1}$), and H is the height of the surface waves (m).

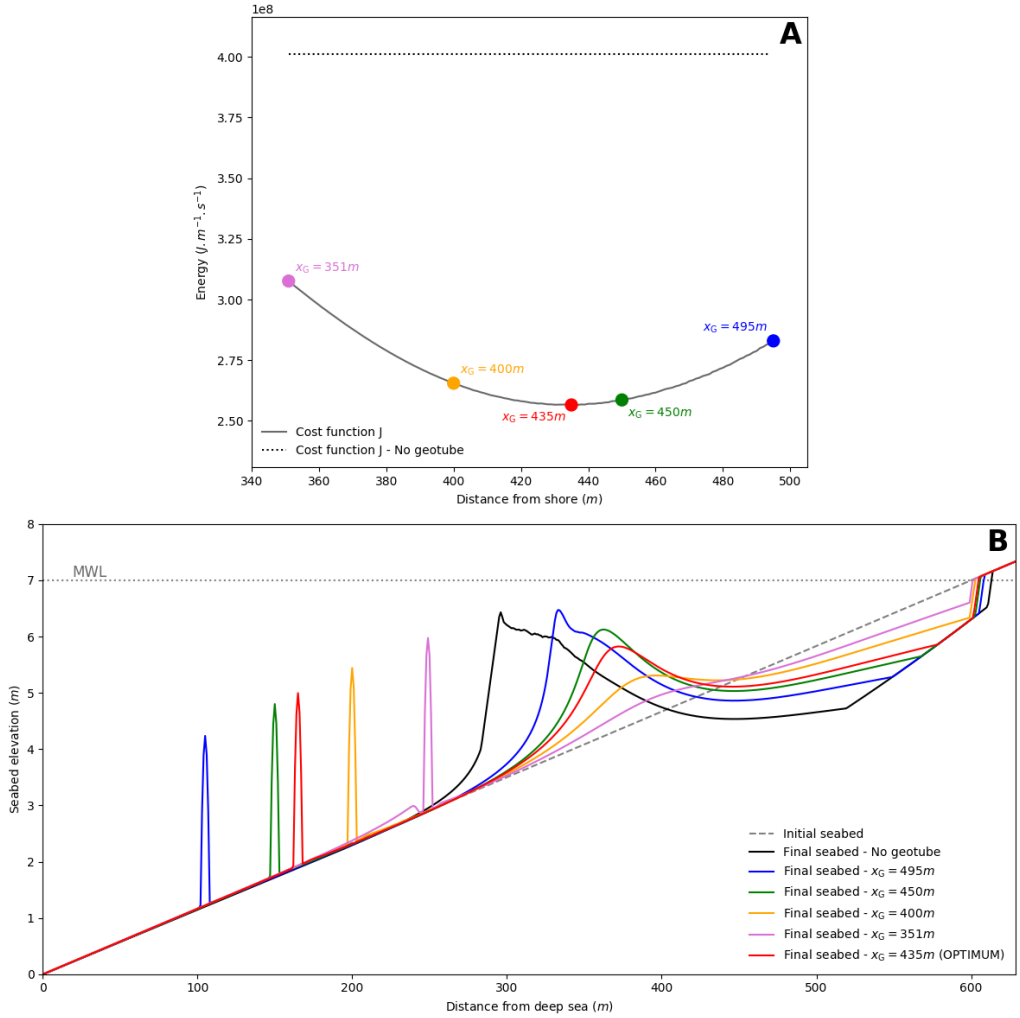

Figure 6: Results of the numerical search of the optimal geotube position via Opti-Morph. **A.** Variations of the geotube deployment objective function with regards to the distance between the geotube and the shoreline. The objective function calculated over a cross-shore profile with geotubes is also given as a reference. Five points are emphasized, corresponding to the five seabeds depicted in the second graphic. **B.** Final seabed profiles produced by the morphodynamic model Opti-Morph with varying geotube positions over the cross-shore profile : $x_G = 495\,m$ (blue), $x_G = 450\,m$ (green), $x_G = 400\,m$ (yellow) and $x_G = 351\,m$ (pink) and the optimal position at $x_G = 435\,m$ (red)

Figure 6.A shows the variations of the objective function $\tilde{\mathcal{J}}_G$ (cf. Eq. (3)) with regard to the location of the geotube. Contrarily to the results

of Section 5.2, a unique minimum is observed at $x_{\mathrm{G}} = 435\,m$ (red point), this signifies that to achieve maximal energy reduction over the course of a storm, the best deployment location of a geotube is at $435\,m$ from the coast. This corresponds to a cumulative wave energy of $2.56 \times 10^8\,J.m^{-1}.s^{-1}$ Other geotube positions are also depicted; their color matching the color of the seabeds in Figure 6.B. The energy associated to a configuration without geotubes is also shown.

Figure 6.B shows the outcome of the seabed, after being subjected to a storm. Six profiles are presented, the same five as in Section 5.2 and the new optimal geotube position $x_{\mathrm{G}} = 435\,m$ (red). As the only difference between this and the previous study is the choice of objective function in geotube location optimization problem, the morphodynamic model produces the same results for the first five seabeds: for $x_{\mathrm{G}} = 495\,m$ (blue), $x_{\mathrm{G}} = 450\,m$ (green), $x_{\mathrm{G}} = 400\,m$ (yellow), and $x_{\mathrm{G}} = 351\,m$ (pink), as well as the configuration without geotube (black). The pink profile was previously featured in red because it corresponded to the optimal position in the previous study. The new addition is the seabed corresponding to the optimal geotube location with regard to wave energy, this is $x_{\mathrm{G}} = 435\,m$ (red). In this configuration, the formation of a sandbar can be observed at $x = 370\,m$, with a height of $1.5\,m$, as well as the creation of a trough whose depth reaches $0.9\,m$, stopped only by the now exposed bedrock. As with the previous study, all geotubes have a position influence on the reduction of wave energy: Figure 6.A shows that for all x_{G}, the associated value of the objective function is less than the energy without geotubes. However, the behavior of the waves and seabed tend towards a configuration without geotube when the geotubes are placed further towards the deep sea.

This study shows that the minimization of erosion of Section 5.2 differs from the minimization of cumulative energy of the waves calculated over the length of the domain. This is due to the manner in which the waves shoal and break. Breaking too early causes a small drop in wave height and thus generates large waves after the geotube. Breaking too late generates large waves prior to breaking at the geotube (with a considerable drop in wave height afterward). As such, the optimal geotube position relative to the energy across the totality of the domain can be found somewhere between these two scenarios.

The rapidity of Opti-Morph and the simplicity of the problem allows the use of a direct method to find the optimal position of the geotube. However, in more complex circumstances, an optimizer may be preferable. By way

of illustration, the Nelder–Mead algorithm [29] was applied to this energy minimization problem, and the minimum of $\tilde{\mathcal{J}}_{\mathrm{G}}$ was found in 20 iterations, which corresponds to a run-time around four times quicker than the direct method.

7. Conclusion

This study was performed in an attempt to demonstrate the potential of the morphodynamic model, Opti-Morph. This model is capable of handling artificial structures such as geotextile breakwaters. We conducted an extensive search for the optimal geotube position, and thus solving two optimization problems simultaneously: the morphodynamic response by wave energy minimization and the optimal geotube position in terms of minimal coastal erosion. Further analyses were conducted to illustrate the influence of the geotube position on the waves. The resulting observations are coherent with expectations, demonstrating the potential of Opti-Morph for coastal engineering projects. In addition to this, Opti-Morph is fast, robust and of low-complexity which makes it an appealing tool for coastal engineering investigations.

References

[1] M. Esteban, H. Takagi, T. Shibayama, Handbook of Coastal Disaster Mitigation for Engineers and Planners, 2015.

[2] R. Cox, D. Beach, Floating breakwater performance - wave transmission and reflection, energy dissipation, motions and restraining forces, Proc 1st Int Conf on the Application of Physical Modeling to Port and Coastal Protection - CoastLab06 (2006) 371–381.

[3] I. Na'im, A. Shahrizal, M. Safari, A short review of submerged breakwaters, MATEC Web of Conferences 203 (2018) 01005.

[4] D. Isèbe, P. Azerad, B. Mohammadi, F. Bouchette, Optimal shape design of defense structures for minimizing short wave impact, Coastal Engineering 55 (2008) 35–46.

[5] M. Cook, F. Bouchette, B. Mohammadi, L. Sprunck, N. Fraysse, Optimal port design minimizing standing waves with a posteriori long term shoreline sustainability analysis, 2021. Preprint.

[6] Y. Xu, Y. Cai, T. Sun, X. Yin, Q. Tan, J. Sun, J. Peng, Ecological preservation based multi-objective optimization of coastal seawall engineering structures, Journal of Cleaner Production 296 (2021) 126515.

[7] J. R. Weggel, N. Rajendran, Optimization of a shore protection scheme for the west coast of india, in: W. Kato, B. C. Gerwick, M. Homma, R. Lenschow, O. T. Magoon, C. C. Mei, S. Motora, K. Okamura, J. Penzien (Eds.), Ocean Space Utilization '85, Springer Japan, Tokyo, 1985, pp. 237–248.

[8] H. Diab, P. Lafon, R. Younes, Optimisation of breakwaters design to protect offshore terminal area, Proceedings of the IASTED International Conference on Modelling, Simulation and Identification, MSI 2014 (2014) 70–75.

[9] G. Elchahal, P. Lafon, R. Younes, Design optimization of floating breakwaters with an interdisciplinary fluid–solid structural problem, Canadian Journal of Civil Engineering 36 (2009) 1732–1743.

[10] E. Castillo, M. A. Losada, R. Mı´nguez, C. Castillo, A. Baquerizo, Optimal engineering design method that combines safety factors and failure probabilities: Application to rubble-mound breakwaters, Journal of Waterway, Port, Coastal, and Ocean Engineering 130 (2004) 77–88.

[11] D. Isebe, P. Azerad, F. Bouchette, B. Ivorra, B. Mohammadi, Shape optimization of geotextile tubes for sandy beach protection, International Journal for Numerical Methods in Engineering 74 (2008) 1262 – 1277.

[12] D. Isèbe, P. Azerad, F. Bouchette, B. Mohammadi, Design of passive defense structures in coastal engineering, International Review of Civil Engineering (IRECE) 5 (2014) 75.

[13] M. Cook, F. Bouchette, B. Mohammadi, S. Meulé, N. Fraysse, OptiMorph, a new platform for sandy beach dynamics by constrained wave energy minimization, 2021. Preprint.

[14] A. Bouharguane, P. Azerad, F. Bouchette, F. Marche, B. Mohammadi, Low complexity shape optimization and a posteriori high fidelity validation, Discrete and Continuous Dynamical Systems-series B - DISCRETE CONTIN DYN SYS-SER B 13 (2010).

[15] B. Mohammadi, A. Bouharguane, Optimal dynamics of soft shapes in shallow waters, Computers and Fluids 40 (2011) 291–298.

[16] A. Bouharguane, B. Mohammadi, Minimization principles for the evolution of a soft sea bed interacting with a shallow, International Journal of Computational Fluid Dynamics 26 (2012) 163–172.

[17] B. Mohammadi, F. Bouchette, Extreme scenarios for the evolution of a soft bed interacting with a fluid using the value at risk of the bed characteristics, Computers and Fluids 89 (2014) 78–87.

[18] C. R. Lawson, Geotextile containment for hydraulic and environmental engineering, Geosynthetics International 15 (2008) 384–427.

[19] R. Koerner, Geotextiles: From Design to Applications, Woodhead Publishing Series in Textiles, Elsevier Science, 2016.

[20] A. Masria, M. Iskander, A. Negm, Coastal protection measures, case study (mediterranean zone, egypt), Journal of Coastal Conservation 19 (2015).

[21] O. Shabankareh, M. Ketabdari, M. A. Shabankareh, Environmental impact of geotubes and geotextiles used in breakwaters and small breakwaters construction (case study: Rigoo public breakwater in south of qeshm island - iran).

[22] I. Alvarez, R. Rubio, H. Ricalde, Beach restoration with geotextile tubes as submerged breakwaters in yucatan, mexico, Geotextiles and Geomembranes 25 (2007) 233–241.

[23] M. González Leija, X. Chavez, E. Alvarez, E. Mendoza, R. Silva, Experimental study on geotextile tube applications as submerged breakwaters for beach protection in yucatan, mexico, Coastal Engineering Proceedings 1 (2014) 25.

[24] Y. Oh, E. Shin, Using submerged geotextile tubes in the protection of the e. korean shore, Coastal Engineering 53 (2006) 879–895.

[25] Y. Oh, E. Shin, J. Kuwano, J. Koseki, Application of submerged geotextile tubes for erosion prevention in east coast of korea.

[26] Y. Balouin, F. Longueville, Y. Colombet, Video assessment of nearshore and beach evolution following the deployment of a submerged geotextile wave breaker, Journal of Coastal Research Special Issue (2016) 617–621.

[27] H. Hidayat, S. Andrianto, Effectiveness of geotextile tubes as a breakwater core, Coastal Engineering Proceedings 1 (2018) 80.

[28] K. Pilarczyk, Design of low-crested (submerged) structures - an overview (2003).

[29] J. A. Nelder, R. Mead, A Simplex Method for Function Minimization, The Computer Journal 7 (1965) 308–313.